International Journal of Architectural, Civil and Construction Sciences
ISSN: 2415-1734
Vol:6, No:7, 2012

Lateral Pressure in Squat Silos under Eccentric Discharge

Y. Z. Zhu, S. P. Meng, W. W. Sun

***Abstract*—**The influence of eccentric discharge of stored solids in squat silos has been highly valued by many researchers. However, calculation method of lateral pressure under eccentric flowing still needs to be deeply studied. In particular, the lateral pressure distribution on vertical wall could not be accurately recognized mainly because of its asymmetry. In order to build mechanical model of lateral pressure, flow channel and flow pattern of stored solids in squat silo are studied. In this passage, based on Janssen's theory, the method for calculating lateral static pressure in squat silos after eccentric discharge is proposed. Calculative formulae are deduced for each of three possible cases. This method is also focusing on unsymmetrical distribution characteristic of silo wall normal pressure. Finite element model is used to analysis and compare the results of lateral pressure and the numerical results illustrate the practicability of the theoretical method.

***Keywords*—**Squat silo, eccentric discharge, lateral pressure, asymmetric distribution

I. Introduction

SILO, plays an important role on numerous agricultural and industrial areas. It is applied on storing, transporting and transferring cereals, coals, cements and so on. Taking its significance into consideration, the designers and constructors of silos pay attention to the safety, reliability, economic and rationality of this kind of structure more and more. However, research on silo seems a challenge to all the scholars. Eccentric discharge effect of the silo is such an item that perplexes many researchers. It is widely recognized to be a much more serious loading condition than concentric discharge or even fully loaded condition. The phenomenon of eccentric discharge is particularly known to be the cause of many catastrophic buckling failures in metal silos in the past. The associated patterns of normal pressures and frictional tractions exerted by the eccentrically flowing stored solids are regarded to produce very asymmetrical patterns of stresses. This non-symmetry in loads causes a bending moment that induces tensile and compressive stresses in the silo wall that can ultimately lead to wall failure.

Y. Z. Zhu is with the Key laboratory of Concrete & Prestressed Concrete Structures of Ministry of Education, Southeast University, Nanjing, 210096, China (phone:+8615151850818; e-mail: trezeguet_zyz@163.com).

S. P. Meng is with the Key laboratory of Concrete & Prestressed Concrete Structures of Ministry of Education, Southeast University, Nanjing, 210096, China (e-mail: cardoso_meng@sina.com).

W. W. Sun is with the Department of Civil Engineering, Nanjing University of Science and Technology, Nanjing, 210094, China (e-mail: sww717@163.com).

The concept about overpressures, which means larger overpressures are generated when silos are unloaded eccentrically, has been also proposed by several research studies. Meanwhile, in order to meet the need of manufacture and transportation, a continued use of eccentric discharge seems inevitable. All these factors indicate that eccentric discharge in silos is an important design aspect which must be taken into account.

Several experiments have been conducted on the eccentric unloading silo since the second half of 20th century (Pieper and Wagner, 1968 [1]; M. L. Reimbert and A. M. Reimbert, 1980 [2]; Pieper *et al*, 1981; Britton and Hawthorne 1984 [3]; Hampe, 1984a, b; McLean and Bravin, 1985 [4]; Ross *et al*., 1980 [5]; Thompson *et al*., 1986, 1988a [6], [7]). At the same time, numerous calculative methods for predicting wall lateral pressure under eccentric unloading were proposed (Jenike, 1967 [8]; Rotter, 1985 [9]; Safarian and Harris, 1985 [10]; McLean and Arnold, 1982; Johnston and Hunt, 1983 [11]; Wood, 1983 [12]; Roberts and Ooms, 1983 [13]; Emanuel *et al*., 1983 [14]; Rotter, 1986 [15]; ACI 313-97, 1997 [16] and Rotter, 2001 [17]). However, assured conclusions are hard to draw through these studies. Either these pressure results are quite distinct from the experimental observations, or these theory resolutions are not always close to each other.

Among these studies, pressure distribution description given by Rotter 1986 [15], who studied eccentric discharge of flat-bottomed silos and suggested actions to calculate wall pressure, illustrated that circumferentially asymmetric pressures simply led to extra circumferential tensions and bending moments. Relevant calculative methods deduced by Rotter are widely recognized and included in BS EN 1991-4 (2006) [18].

In Rotter's (1986) theory and BS EN 1991-4 (2006), the flow channel and pressure pattern is clearly described. A non-uniform pressure distribution is specified on the silo wall circumference for eccentric discharging silo. This pressure distribution is a function depending on the silo slenderness, its diameter and the eccentricity of the discharge outlet. In regard to the flow channel, it suggests that the geometry of the flow channel cannot be directly deduced from the discharge arrangements and silo geometry, and no less than three values of the radius of flow channel are taken to tentative calculate. Because of its special overall flowing pattern, slender silo has a varied flow channel, whereas Rotter's theory is fit for calculating pressure distribution of slender silos.

The key problem is that the squat silo's tubular flowing pattern, which differs from that of slender silo, makes Rotter's

theory unsuitable for predicting wall pressure in squat silos, for that the flow channel is relevant fixed when the geometry of the silo and the outlet is determined. Moreover, upper cone-shaped stored solids above the supine surface of squat silo takes an important impact on the wall pressure. Some simplification like that made in the slender silo seems inaccurate. In this paper, the Janssen's theory [19] is treated as the base, the calculation procedure suitable for squat silos is proposed. And then a simple squat silo, generally a reinforced concrete silo, is given to assess its wall pressure by method described in this paper. The finite element method (FEM) and the commercial finite-element program ANSYS 10.0 is used to analysis the load actions on structural. The comparison between theoretical and FEM results would illustrates the reliability of this set of calculative method introduced in this story.

II. Flowing Pattern in Squat Silos

The calculation about wall pressures under eccentric discharge relates to a flowing pattern, for that the flow pattern influences the distribution of stored solids in silos and in turn affects the pressures exerted by both the static and flowing solid components on the silo wall. Meanwhile, the aspect ratio of the silo is considered to have an important influence on the possible patterns of flowing (Fig. 1). Considering that squat silos having significantly different pipe flow regimes from slender ones, mechanical model of wall pressure calculation about squat silos would be distinct from that about slender ones [20].

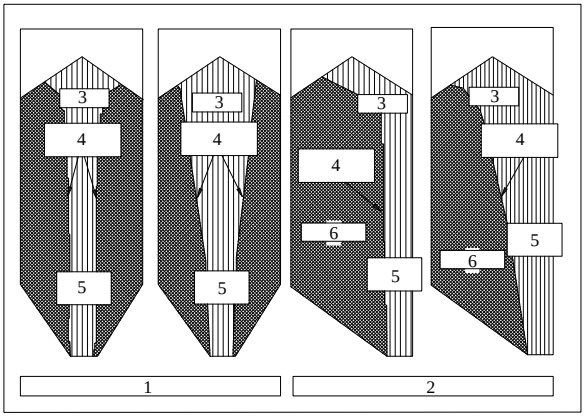

(a) Parallel pipe flow (b) Taper pipe flow (c) Eccentric parallel pipe flow (d) Eccentric taper pipe flow

Key:
1 Internal pipe flow
2 Eccentric pipe flow
3 Flowing
4 Flow channel boundary
5 Flowing pipe
6 Stationary

Fig. 1 Pipe flow patterns

According to Rotter's (1986) theory, eccentric discharge pressure pattern in a slender silo is based on a parallel-sided flow channel which is actually cylindrical surface throughout the height of the silo (Fig. 2(a)).

Also this channel that is assumed to contact with the wall of silo leads to a corresponding frictional traction. Whereas in a squat silo, the flowing regime is relevantly limited and its dimension is fixed when the geometry of silo, especially outlet, is determined.

The assumption in a slender silo that the flowing channel is in touch with the silo wall is unsuitable for that in a squat silo. When the flowing happens in the region inside the silo as well the stored solids adjacent to the silo wall stay static (Fig. 2(b)), flowing part of stored solids would have a limited influence on the variation of fractional traction of silo wall. The imbalance of vertical friction forces caused by differences in static and dynamic coefficients of friction combined with the asymmetric geometry generated by eccentric discharge is not obvious in a squat silo wall [21]. And this friction imbalance generated inside the flowing channel during eccentric unloading has little influence on the overall silo wall pressure due to its limited dimension of the channel. Considering all these factors, wall pressure calculation in squat silos would focus on static pressure when eccentric discharge suspends. The appearance and distribution of stored solids inside the silos seems crucial for building mechanical model.

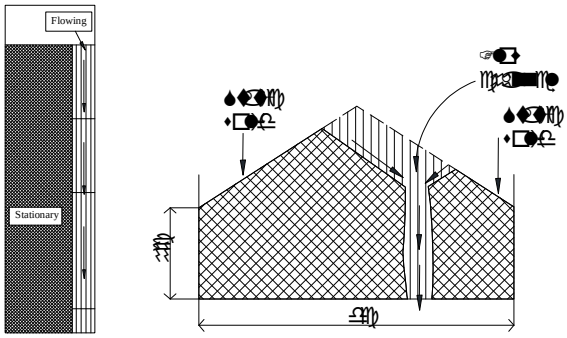

(a) (b)

Fig. 2 Eccentric discharge flow model

III. Wall Pressures Calculation

A. Calculation Assumptions

Three basic assumptions are made when deducing the calculative method of lateral pressure for squat silos under eccentric discharge:

1) The discharge outlet at the flat-bottom is a single circular orifice. At the surface of stored solids, there forms an inverted cone whose vertex is dead against the center of the outlet.

2) The included angle between discharge surface and horizontal plane equals the angle of repose of the stored materials.

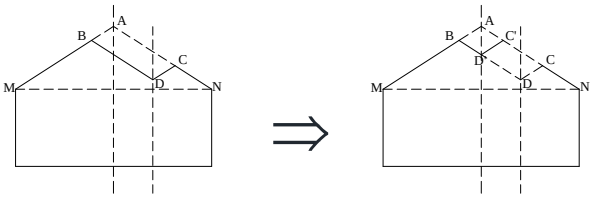

Fig. 3 Model of simplified calculation

3) When addresses the wall pressure in the place of point *M*,

it is assumed that pressure under eccentric discharge is approximate to that under concentric discharge. As is shown in Fig. 3, part of stored solids (*C'CDD'*) is added to calculate wall pressure of point *M*. However, the influence of this part of stored solids is limited; moreover, this approximation is advantageous to the design of silos.

B. Pressure in the Wall

According to different discharge stages, three possible cases are considered in this passage and these cases are classified by different geometrical relationships among discharge surface, static stored solids, and wall of silos.

1) Case 1

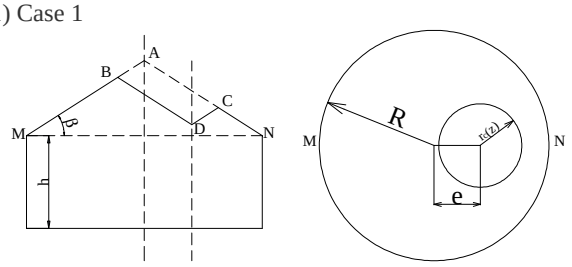

(a) (b)

Fig. 4 Model of case 1

In this case, the vertex (*D'*) of the transferred discharge surface, which is conical, shown in Fig. 3, is still above the supine surface (*MN*) of the silo. The surface *DBC* shown in Fig.4 (a) is actually a conical surface and this curved surface intersects with the conical surface *AMN* and points *B* and *C* lie in the line of intersection.

As general practice, it is assumed that the horizontal pressure *p* is relatively constant surround the silo wall, the ratio of the horizontal pressure on the wall to the mean vertical stress in the stored solid *q* is simply defined by the parameter *K*, which is taken as a material constant.

The equation of vertical equilibrium of a slice throughout the silo section may may be written:

$$qA + \gamma A dz = A\left(q + \frac{dq}{dz}dz\right) + \mu' p\left(Udz\right) \qquad (1)$$

Where:

- γ is the unit weight of the stored solid;
- μ' is the wall friction coefficient for solid against the cylindrical wall;
- U is the perimeter of cylindrical silo wall.

The solution to (1) would give Janssen's equation for the horizontal pressure at depth z:

$$p = \frac{\gamma\rho}{\mu'} + C_1 K e^{-\frac{\mu' K z}{\rho}} \qquad (2)$$

Where:

- ρ is the hydraulic radius of silo, equals sectional area divided by perimeter of cylindrical silo wall;
- C_1 is the arbitrary constant.

According to the vertical equilibrium of stored solids above the supine surface of the silo, the boundary condition that the mean vertical stress at the height of zero could be written:

$$q(0) = \frac{\gamma \Delta V}{A_0} \qquad (3)$$

Here, the geometry of section is shown in Fig. 4, the angle of response is defined by β and the vertical distance from the vertex of *D* to the supine surface is set as h_D.

The expression about the volume of remanent stored solids above the supine surface of silo is:

$$\Delta V = \frac{\pi \tan\beta}{3}\left[R^3 - \frac{1}{4}\left(\cot\beta \cdot h_D + e - R\right)^3\right] \qquad (4)$$

and the sectional area at the height of zero is:

$$A_0 = \pi R^2 \qquad (5)$$

Subject to the boundary, the constant C_1 in (2) may be solved as:

$$C_1 = \gamma\left[\frac{\tan\beta}{24R^2}\left(\cot\beta \cdot h_D + e - R\right)^3 - \frac{\rho}{\mu' K}\right] \qquad (6)$$

2) Case 2

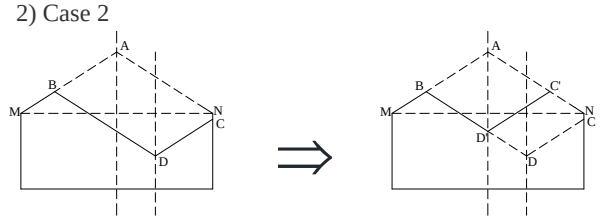

Fig. 5 Model of case 2

In this case, the vertex of the transferred discharge surface (*D'*), shown in Fig. 5, is below the supine surface (*MN*) of the silo whereas part of stored solids surpluses above the supine surface of the silo.

The volume of remanent stored solids above the supine surface of silo is:

$$\Delta V = \frac{\pi \tan\beta}{3}\left[R^3 - \frac{1}{4}\left(\cot\beta \cdot h_D + e - R\right)^3 + \left(h_D \cot\beta - e\right)^3\right] \qquad (7)$$

and also the sectional area at the height of zero is as:

$$A_0 = \pi\left(R^2 - h_D^2 \cot^2\beta\right) \qquad (8)$$

When the calculative height satisfies $0 \le z \le h_D - e\tan\beta$, then the equation of equilibrium would be written as:

$$qA(z) + \gamma dV = A(z+dz)(q + \frac{dq}{dz}dz) + \mu' p\left(Udz\right) \qquad (9)$$

The expression of sectional area would be an equation of the height *z*:

$$A(z) = \pi R^2 - \pi(h_D - e\tan\beta - z)^2 \cot^2\beta \qquad (10)$$

According to the Taylor's formula, the expression of sectional area would be simplified as:

$$A(z+dz) = A(z) + A'(z)dz + A''(z)(dz)^2 \qquad (11)$$

and the differentiation of volume would be expressed as:

$$dV = \int_z^{z+dz} A(z)dz \qquad (12)$$

Using (11) and (12), (9) would be stated as follows:

$$\pi\left(\gamma-\frac{dq}{dz}\right)(R^2-(h_D-e\tan\beta-z)^2\cot^2\beta)$$
$$=-2\pi(h_D-e\tan\beta-z)\cot^2\beta\cdot q+K\mu'U\cdot q \tag{13}$$

The equation of solution to (13) would be:

$$q=\frac{\gamma}{\lambda_1}+C_{21}e^{-\lambda_1} \tag{14}$$

Where:

λ is the parameter defined as:

$$\lambda_1(z)=\ln\left[R^2(1-\cos 2\beta)-(h_D-e\tan\beta-z)^2(1+\cos 2\beta)\right]$$
$$+\frac{K\mu'U\cdot\operatorname{arctanh}[\frac{(h_D-e\tan\beta-z)\cot\beta}{R}]\cdot\tan\beta}{\pi R} \tag{15}$$

Also, the boundary condition of the vertical stress q is:

$$q(0)=\frac{\gamma\Delta V}{A_0} \tag{16}$$

When satisfying the boundary, the constant C_{21}in (2) may be solved as:

$$C_{21}=\gamma\left(\frac{\Delta V}{A_0}-\frac{1}{\lambda_1(0)}\right)e^{\lambda_1(0)} \tag{17}$$

The vertical stress at the height of h_D would be:

$$q(h_D)=\frac{\gamma}{\ln\left[R^2(1-\cos 2\beta)\right]}+\left(\frac{\Delta V}{A_0}-\frac{1}{\lambda_1(0)}\right)\frac{\gamma e^{\lambda_1(0)}}{R^2(1-\cos 2\beta)} \tag{18}$$

When the height meets with $h_D-e\tan\beta\le z\le h$, the expression about pressure p may be written as:

$$p=\frac{\gamma\rho}{\mu'}+C_{22}Ke^{-\frac{\mu'Kz}{\rho}} \tag{19}$$

Using (18) as the boundary condition, the constant C_{22} in the pressure equation (19) would be solved:

$$q\Big|_{z=h_D-e\tan\beta}=q(h_D-e\tan\beta) \tag{20}$$

$$C_{22}=\left[q(h_D-e\tan\beta)-\frac{\gamma\rho}{\mu'K}\right]\cdot e^{\frac{\mu'K(h_D-e\tan\beta)}{\rho}} \tag{21}$$

3) Case 3

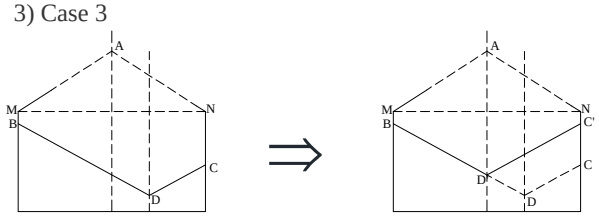

Fig. 6 Model of case 3

In this case, the vertex of the transferred discharge surface cone (D'), shown in Fig. 6, is below the supine surface (MN) of the silo and the highest point (B) is below the supine surface.

When the height belongs to $0\le z\le h_D-e\tan\beta$, then:

$$q(z)=\frac{\gamma}{\lambda_2}+C_{31}e^{-\lambda_2} \tag{22}$$

Where:

$$\lambda_2(z)=\ln\left[R^2(1-\cos 2\beta)-(R\tan\beta-z)^2(1+\cos 2\beta)\right]$$
$$+\frac{K\mu'U\cdot\operatorname{arctanh}\left(1-\frac{z\cot\beta}{R}\right)\cdot\tan\beta}{\pi R} \tag{23}$$

According to the boundary condition:

$$q(0)=0 \tag{24}$$

$$C_{31}=\frac{\gamma e^{\lambda_2(0)}}{\lambda_2(0)} \tag{25}$$

$$q(h_D-e\tan\beta)=\frac{\gamma}{\ln R^2(1-\cos 2\beta)}+\frac{\gamma e^{\lambda_2(0)}}{R^2\lambda_2(0)(1-\cos 2\beta)} \tag{26}$$

When the height meets with $z\ge h_D-e\tan\beta$, the

$$q=\frac{\gamma\rho}{\mu'K}+C_{32}e^{-\frac{\mu'Kz}{\rho}} \tag{27}$$

$$C_{32}=(q(h_D-e\tan\beta)-\frac{\gamma\rho}{\mu'K})\cdot e^{\frac{\mu'K(h_D-e\tan\beta)}{\rho}} \tag{28}$$

C. Circumferentially non-uniform pressures distribution

Both the pressures in bottom of the silo of point M and N could be calculated by the formulae deduced above which are defined as $p(M)$ and $p(N)$. It is assumed that the value of pressure about each point surround the circle relates to the height of stored solids of each point, therefore the equation would be expressed as:

$$\frac{p(M)}{p(N)}=\left(\frac{h(M)}{h(N)}\right)^{\alpha} \tag{29}$$

Where:

$h(M)$ is the height of highest point of stored solids
$h(N)$ is the height of the point C, shown in Fig. 4

The coefficient α may be determined by the aspect ratio of the silo, the property of the stored solids and other factors, and the value of α would close to 0.5. In this passage, a simplified suggestion for the value of α is 0.5, then:

$$\frac{p(M)}{p(N)}=\sqrt{\frac{h(M)}{h(N)}} \tag{30}$$

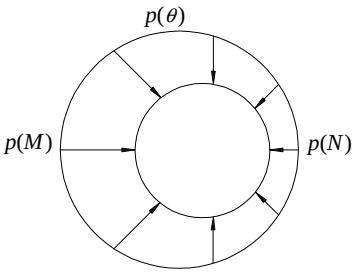

Fig. 7 Circumferential pressure distribution

It is supposed that the pressure distribution principle, shown in Fig.7, on the circumference could be expressed as follows:

$$p(\theta) = p(M)\sqrt{\frac{h(\theta)}{h(M)}} \tag{31}$$

Where:

$p(\theta)$ is the pressure of circumferential distribution;
$h(\theta)$ is the height of the each point on the intersection, shown in Fig. 4;
θ is the central angle.

In order to deduce the expression of $h(\theta)$, three different cases are also specified, shown in Fig. 8.

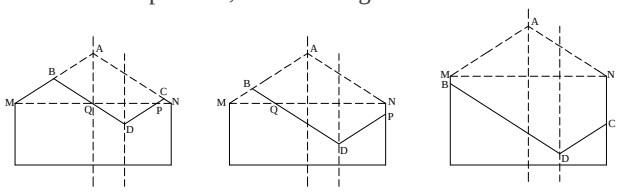

Fig. 8 Height of stored solids

If both of the points B and C are above the supine surface, the expression about $h(\theta)$ would be:

$$h(\theta) = \frac{-(R\tan\beta)^2 + h_D^2 + e\tan^2\beta(2R\cos\theta - e)}{2(-R\tan\beta \pm h_D + e\cos\theta\tan\beta)} + h \tag{32}$$

If the point B is above the supine surface, whereas the point C is below that plane, the expression about $h(\theta)$ would be:

$$h(\theta) = \begin{cases} \dfrac{-(R\tan\beta)^2 + h_D^2 + e\tan^2\beta(2R\cos\theta - e)}{2(-R\tan\beta + h_D + e\cos\theta\tan\beta)} + h \\ \tan\beta\sqrt{(R\cos\theta)^2 + (R\sin\theta + e)^2} - h_D + h \end{cases} \tag{33}$$

As is shown in Fig. 8, when both of the point B and C are below the supine surface, the $h(\theta)$ would be written as:

$$h(\theta) = \tan\beta\sqrt{(R\cos\theta)^2 + (R\sin\theta + e)^2} \pm h_D + h \tag{34}$$

IV. EXAMPLE ANALYSIS

A. Model generation

For analyzing the static pressures, interaction of concrete walls, elasto-plastic behavior of the stored solids, and the structure consequences in a cylindrical concrete silo with a flat-bottom companying with an eccentric outlet, a typical silo is designed, and the dimensions of which is shown in Fig.9.

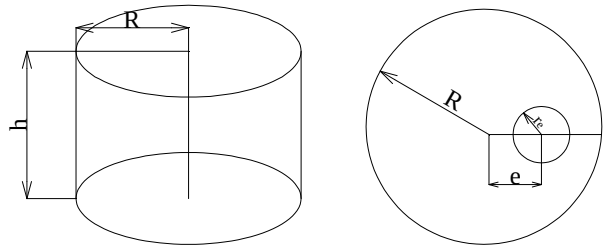

Fig. 9 Dimensions of the silo model

The silo with height 30 m and a radius of 20 m had an aspect ratio of 0.75 which is classified as squat silo. The eccentricity e of the discharge outlet center is 10 m. Here, the dimension of the flowing channel is neglected for that in the static pressure analysis procedure the radius of the discharge outlet has no influence on the distribution of stored solids when the discharge has been suspended.

B. Numerical model

The eight-node SHELL 93 element was selected to model the wall of silo, and the thickness of the shell was defined to 400mm. Eight-node SOLID65 element was used to simulate the stored material. In order to model such particulates inside the silo, the elasto-plastic criterion by Drucker-Prager (DP) has been applied to SOLID65 element [22]-[25].

Contact element was utilized to consider interaction between silo wall and stored material. 3-D eight-node Surface-to-Surface CONTA 173 and 3-D target segment TARGE170 were applied to couple field contact analyses. Selected areas of the silo wall were meshed with the TARGE 170 element. Then the areas of stored solids were selected and meshed with the CONTA 173 element, placing the nodes of those elements over the faces of the SOLID 65 elements in contact with the wall.

Referring to the definition of the model variables, three plastic parameter values necessary for the development of the Drucker-Prager criterion were introduced: cohesion, internal friction angle, and dilatancy angle, the elastic parameters necessary for the elastic part of the behavior of the material were also presented: Young's modulus and Poisson's ratio, listed in Table. I.

TABLE I
PARAMETER VALEUES FOR NUMERICAL MODEL

Property	Value
Unit weight, γ (kN/m^3)	16.0
Young's modulus, E (MPa)	10.0
Poisson's ratio, ν	0.32
Cohesion, C (MPa)	0
Internal friction angle, Φ (。)	33
Dilatancy angle, φ (。)	33
Coefficient of friction with the wall, μ	0.5

The nodes of shell elements at the base of the silo associating with those of solid elements were anchored to the foundation, which was simulated as fixed. All the degrees of freedom of the nodes at the bottom combining with the

foundation were constrained (shown in Fig. 12). The silo wall meshed model solely without constraints is shown in Fig. 10. Fig. 11 represents silo wall model in company with stored solids model, also without constraints. Fig. 12 indicates restrained wall model that has been meshed.

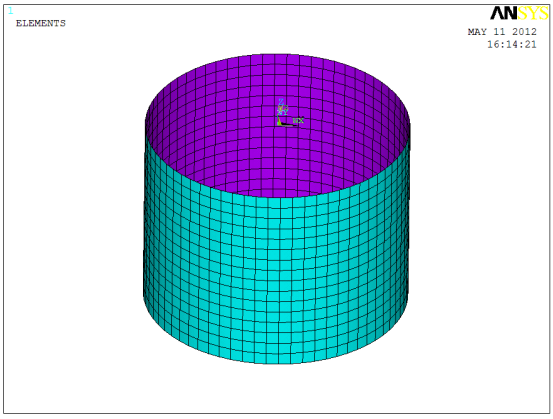

Fig. 10 Silo wall meshed model without constraint

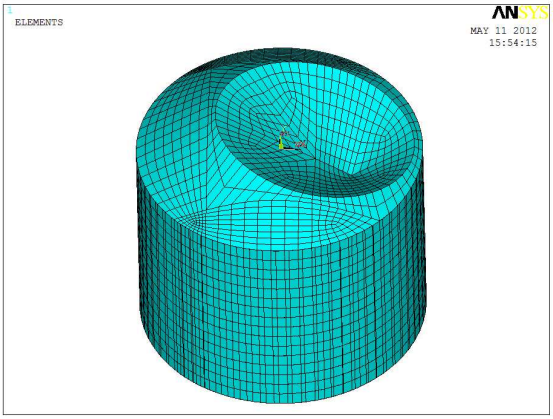

Fig. 11 Stored solids meshed model

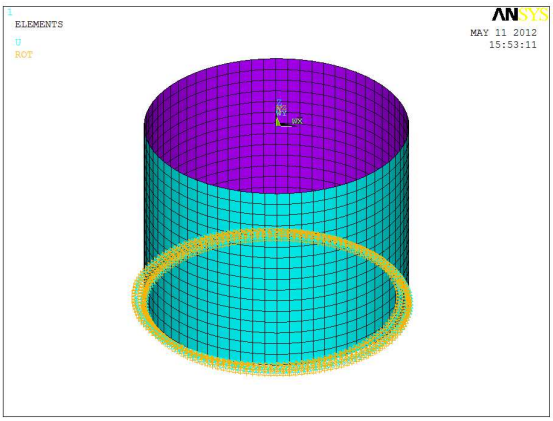

Fig. 12 Silo wall meshed model with constraint

C. Vertical pressure results analysis

Fig. 13 shows the distinction about the values of normal pressures which are obtained from different methods. Analyzing the pressure results on top and on the both sides of cylindrical wall, the results got through theoretical method, which base on Janssen's 1895 theory present a tendency for normal pressures that are very similar to the results obtained from FEM. According to the FEM analysis, closing to the bottom part of the silo, pressures decrease after they reached the maximum value. At the bottom of silo, pressures got from FEM are generally smaller when compared to those from theoretical method. Different from the varied principle of lateral pressure on vertical direction got from FEM, principle of theoretical results presents a continuously increased tendency.

For the first state which is the incipient stage of discharge, Fig. 13 (a) shows an approximately symmetrical characteristic about the distribution of lateral pressure. The FEM and theoretical results are fit close to each other especially at the top of the silo. According to the FEM results, pressures at the height of about 25 m reach their maximum with the values of 153 kPa and 143.89 kPa. What the largest value for theoretical results are 166.04 kPa and 161.80 kPa at the base of silo. Being worth mentioning is that at the top of the silo that the vertical coordinate is zero, these normal pressures did not equal to zero, which illustrates that the equivalent surface above the top face of silo is necessary for calculating the normal pressure.

For the second state, the pressures of left side have the similar varied tendencies compared to those at the first state. However, at the right side of the Fig. 13 (b), pressures were about zero at the height of 4 m, meanwhile, at the range of 0 to 4 m, stored solids exert no normal pressure to the silo wall. From this state, the pressure curve began to present obvious difference between two sides of the figure mainly because of the asymmetry of stored solids between two sides of silo center inside the silo. According to theoretical method, maximum pressures of two sides are 107.63 kPa and 92.49 kPa whereas the FEM results show two maximum values at 115.9 kPa and 108.55 kPa.

The most distinct characteristic of pressure curve about the third state differs from the first two states is that at the left side of Fig. 13 (c), the pressure at the top face of silo was zero, for that with the proceeding of eccentric discharge, stored solids there has dropped below the height of 2 m.

For the fourth state, the non-symmetry of two sides' pressures was more apparent than another three states. According to the theoretical results, the ratio of the maximum pressure at the left side to that at the right side is 1.54 whereas the ratios of the other three states are 1.026, 1.164, and 1.407.

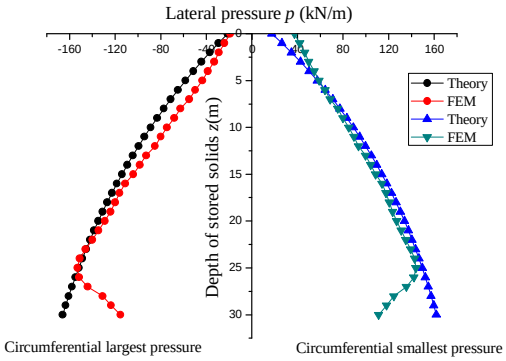

(a) State 1

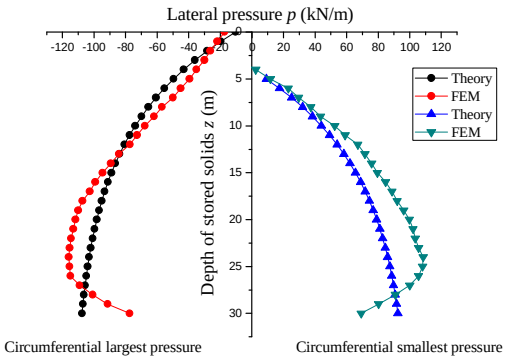

(b) State 2

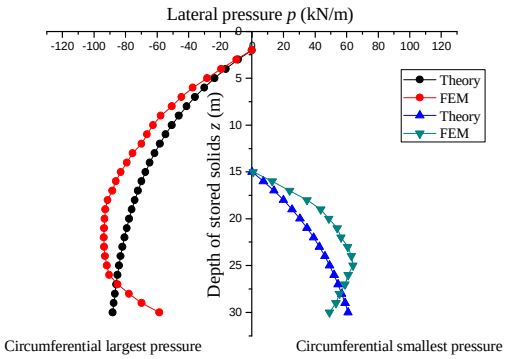

(c) State 3

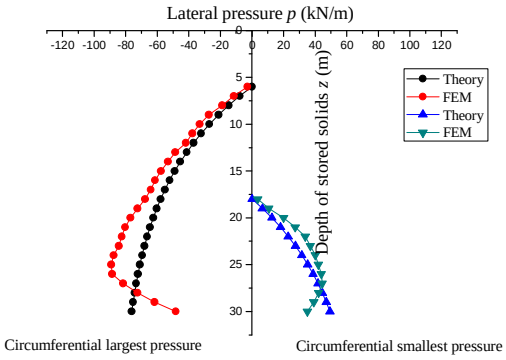

(d) State 4

Fig. 13 Vertical lateral pressure comparison under different discharge stages

D. Circumferential pressure results analysis

Fig. 14 shows the comparison between the FEM and the theoretical results about the circumferential pressure distribution. Two curves in each figure seem fit close to each other, illustrating that the calculative formula (31) suggested in this passage is practicable. However, small disparity was existent and the improved measure would be that revising the coefficient α proposed in (29).

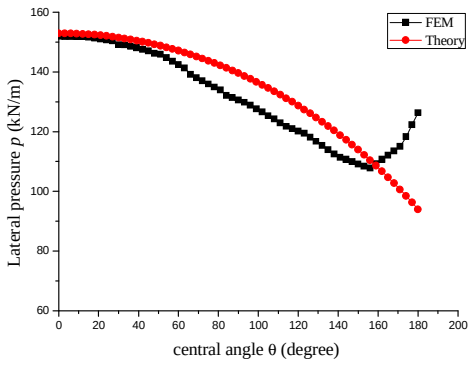

(a) State 1

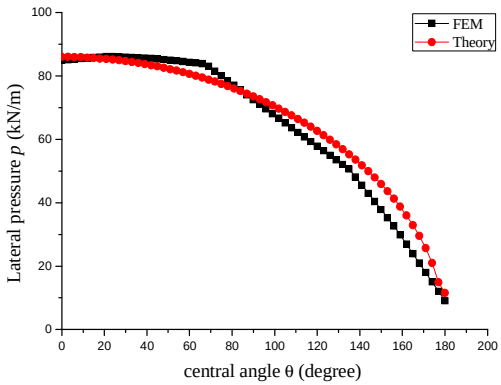

(b) State 2

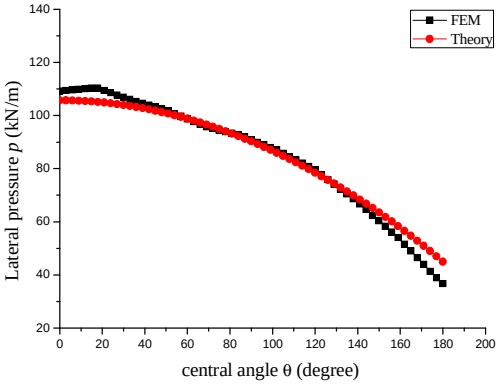

(c) State 3

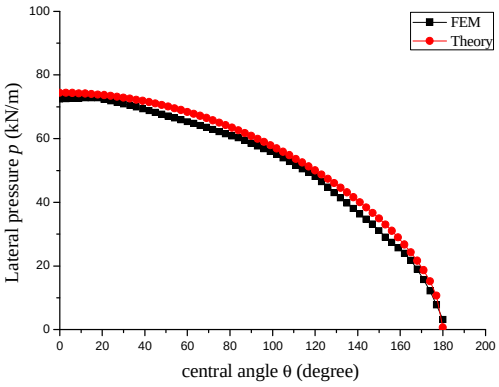

(d) State 4

Fig. 14 Circumferential lateral pressure comparison under different discharge stages

V. Conclusion

The following conclusions are based on the study:

1) This story has focused on the flowing pattern of squat silos. In accord to its particular filling style and discharge pattern, the squat silo has a flowing channel with fixed dimension. Owing to its flowing channel keeping away from the silo wall, flowing solids bring limited imbalance friction force for the silo wall so that this imbalance of vertical friction force caused by differences in static and dynamic of friction could be neglected.

2) For simplifying the process of building mechanical and mathematical model, three assumptions are made. Regarding the Janssen's (1895) theory as the basic, mechanical equilibrium was built for calculation of lateral pressure in squat silos under eccentric discharge. Considering different geometrical relationships between stored solids and silo wall, this story has drawn three cases. Pressure calculative formulae for each case are delicately deduced according to equilibrium inside the silo at any level.

3) The notable feature of the distribution on normal pressure under eccentric unloading is circumferential non-symmetry. This paper has paid attention to the pressure pattern in squat silos and proposed relevant calculative method. This theoretical method based on the assumption that circumferential normal pressure related to the peak height of stored solids of each point on the circumference. Pressure distribution prediction at any level could be accomplished through proposed formulae.

4) Finite element model that modeled eccentric discharge on static conditions has been built through ANSYS. Contact analysis and non-linear analysis are directed to reflect the interaction between stored solids and silo wall.

5) A close fit was found through results comparison between FEM and theoretical results on vertical pressure. However, at the bottom zone of the silo, the vertical pressure curves had two different shapes, showing the deviations between the theory and FEM about the pressure analysis. This is because the inherent defect of Janssen's theory that leads this inaccuracy. What was the limitation is that Janssen's theory could not take the boundary condition at the bottom of the silo into account, whereas constrains at the base of silo significantly influence the distribution of vertical pressure.

6) Some reasonable fitting results of the comparison of FEM and theoretical resultants about circumferentially normal pressure were shown in this passage. Theoretical method proposed in this story seemed rational according to the example analysis. Nevertheless, some adjustments would be done to adopt the FEM results and even experimental results better.

References

[1] Pieper, K., and Wagner, K., "The influence of different types of discharging on side pressures in silo compartments," *Aufbereitungs-Technik*, vol. 10, pp. 542-546, 1969. (in German).

[2] Reimbert, A. M., and Reimbert, M. L., "Pressure and overpressures in vertical and horizontal silos," *Proceedings of the International Conference on Design of Silos for Strength and Flow*, University of Lancaster, 1980, pp. 364.

[3] Britton, M. G., and Hawthorne, C. R. J., "Dynamic behavior of wheat in a lamellar bin," *Amer. Soc. of Agric. Engrs.*, vol. 84, pp. 501, 1984.

[4] McLean, A. G., and Bravin, B., "Wall loads in eccentric discharge silos," *Int. J. Bulk Solids Storage in Silos*, vol. 1, no. 1, pp. 12-24, 1985.

[5] Ross, I. J., Moore, D. W., Loewer, O. J., and White, G. M., "Model studies of grain silo failures," *Winter Meeting*, Amer. Soc. Agric. Engrs., Chicago, 1980, pp. 2-264.

[6] Thompson, S. A., Usry, J. L., and Legg, J. A., "Loads in a model grain bin as affected by various unloading techniques," *Trans., Amer. Soc. Agric. Engrs.*, vol. 29, no. 2, pp. 556-561, 1986.

[7] Thompson, S. A., Usry, J. L., and Morse, D. D., "Experiments with the eccentric unloading of a model corrugated grain bin," *Canadian Agric. Engrg.*, vol. 30, no. 1, pp. 165-171, 1988a.

[8] Jenike, A. W., "Denting of circular bins with eccentric drawpoints," *ASCE J. Struct. Div.*, vol. 93, no. 1, pp. 27-35, 1967.

[9] Rotter, J. M, "Buckling under axial compression," *Design of Steel Bins for the Storage of Bulk Solids*, J. M. Rotter, ed., Sydney: The Univ. of Sydney School of Civ. and Mining Engrg., pp. 122-137, 1985.

[10] Safarian, S. S., and Harris, E. C., *Design and construction of silos and bunkers*, N.Y.: Van Nostrand Reinhold Co., 1985.

[11] Johnston, F.T. and Hunt, F.A., "Solutions for silo asymmetric flow problems," *Proc., Second Int. Conf. on Design of Silos for Strength and Flow*, Stratford-upon-Avon, 1983, pp. 13.

[12] Wood, J. G. M., "The analysis of silo structures subject to eccentric discharge," *Proc., Second Int. Conf. on Design of Silos for Strength and Flow*, Stratford-upon-Avon, 1983, pp. 44.

[13] Roberts, A. W., and Ooms, M., "Wall loads in large metal and concrete silos and silos due to eccentric draw-down and other factors," *Proc., Second Int. Conf. on Design of Silos for Strength and Flow,*

Stratford-upon-Avon, 1983, pp. 70.

[14] Emanuel, J. H., Best, J. L., Mahmoud, M. H., and Hasanain, G. S., "Parametric study of silo- material interaction," *Powder Tech.*, vol. 36, pp. 223-33, 1983.

[15] Rotter, J. M., "The analysis of steel bins subject to eccentric discharge," *Proc., Second Int. Conf. Bulk Materials Storage Handling and Transportation*, Wollongong, 1986, pp. 264-271.

[16] ACI 313-97, *Standard practice for design and construction of concrete silos and stacking tubes for storing granular materials.* Detroit: ACI, 1997, pp. 6-8.

[17] Rotter, J. M., "Pressures, stresses and buckling in metal silos containing eccentrically discharging solids," *Festschrift Richard Greiner, celebration volume for the 60th birthday of Prof. Richard Greiner*, TU Graz, Austria, 2001, pp. 85–104.

[18] EN 1991-4. *Eurocode 1: actions on structures, Part 4: silos and tanks*. Brussels: European Committee for Normalisation, 2006, pp. 40-65.

[19] Janssen, H. A., "Versuche uber getreidedruck in silozellen," *Zeitschrift des Verein Deutscher Ingenieure*, vol. 39, pp. 1045-1049, 1895. (in German).

[20] A. J. Sadowski, J. M. Rotter, "Steel silos with different aspect ratios: II— behaviour under eccentric discharge," *Journal of Constructional Steel Research*, vol. 67, no. 10, pp. 1545-1553, 2011.

[21] R. A. Bucklin, S. A. Thompson, and I. J. Ross, "Bin-wall failure caused by eccentric," *Journal of Structural Engineering*, vol. 116, no. 11, pp. 3175-3190, 1990.

[22] E. Gallego, C. González-Montellano, A. Ramírez, F. Ayuga, "A simplified analytical procedure for assessing the worst patch load location on circular steel silos with corrugated walls," *Engineering Structures*, vol. 33, pp. 1940-1954, 2011.

[23] P. Vidal, A. Couto, F. Ayuga, and M. Guaita, "Influence of hopper eccentricity on discharge of cylindrical mass flow silos with rigid walls," *ASCE Journal of Engineering Mechanics*, vol.132, no. 9, pp. 1026-1033, 2006.

[24] F. Ayuga, M. Guaita, P. J. Aguado, and A. Couto, "Discharge and the eccentricity of the hopper influence on the silo wall pressure," *ASCE Journal of Engineering Mechanics*, vol.127, no. 10, pp. 1067-1074, 2001.

[25] M. Guaita, A. Couto, F. Ayuga, "Numerical simulation of wall pressure during discharge of granular material from cylindrical silos with eccentric hoppers," *Biosystems Engineering*, vol. 85, no. 1, pp. 101-109, 2003.